JTTEE5 22:646–658
DOI: 10.1007/s11666-013-9889-8
1059-9630/$19.00 © ASM International

Plasma-Sprayed Thermal Barrier Coatings: New Materials, Processing Issues, and Solutions

Georg Mauer, Maria Ophelia Jarligo, Daniel Emil Mack, and Robert Vaßen

(Submitted October 12, 2012; in revised form January 2, 2013)

Growing demands on thermal barrier coatings (TBCs) for gas turbines regarding their temperature and cyclic capabilities, corrosion resistance, and erosion performance have instigated the development of new materials and coating systems. Different pyrochlores, perovskites, doped yttria-stabilized zirconia, and hexaaluminates have been identified as promising candidates. However, processing these novel TBC materials by plasma spraying is often challenging. During the deposition process, stoichiometric changes, formation of undesired secondary phases or non-optimum amorphous contents, as well as detrimental microstructural effects can occur in particular. This article describes these difficulties and the development of process-related solutions by employing diagnostic tools.

Keywords hexaaluminate, particle diagnostics, perovskite, plasma spraying, pyrochlore, thermal barrier coating, yttria-stabilized zirconia

1. Introduction

In modern gas turbines, plasma-sprayed thermal barrier coating (TBC) systems have been applied for several decades to improve performance (Ref 1-3). The thermally insulating layer can reduce the temperature of the metallic substrate resulting in improved component durability. Furthermore, an increase in efficiency can be achieved by permitting an increase of the turbine inlet temperatures. Thus, TBCs offer great benefits for the operation of aircraft gas turbine engines, shipboard gas turbine engines, and land-based industrial gas turbine engines.

Presently, research on TBCs is facing new demands. Coatings are needed for resisting degradation induced by environmental air-borne deposits ingested into the engine especially in the case of aircraft gas turbine engines where in-take air filtration is not possible. The so-called CMAS (which stands for calcium-magnesium-aluminum-silicate) attack is caused by the deposition of glass-forming constituents and infiltration above the melting temperature of the glass phases (Ref 4). At solidification, large parts of the TBC spall off because of the considerable loss of strain tolerance of the glass phases. Presently, anti-CMAS approaches under investigation aim to induce early crystallization to stop infiltration by dopants, such as dissolved Al, Ti, or Gd (Ref 5, 6).

Another demand of future TBCs is to provide fuel flexibility. New problems limiting component life occur because of higher temperatures and new combustion gases (syngas, hydrogen, or natural gas contaminants (Ref 7)) causing overheating and hot corrosion (Ref 8). Currently, research activities are undertaken to understand dominant damage mechanisms and to identify cost-effective alternatives for materials and coating technologies.

TBC systems are complex, multilayered, and multimaterial systems with many variants related to composition, processing, and microstructure. They consist of at least two layers: a bondcoat layer, and an insulating ceramic topcoat. The bondcoat is often a metal and has two major functions: it improves bonding between the substrate and the topcoat, and it protects the substrate from corrosion and oxidation. The ceramic topcoat provides heat insulation by its low thermal conductivity resulting from bulk material characteristics as well as from microstructural features such as pores and voids.

In terms of deposition techniques, two methods have become well established. One is electron beam-physical vapor deposition (EB-PVD), and the other is atmospheric plasma spraying (APS). Coatings deposited by EB-PVD have specifically columnar microstructures (Ref 9) and are mainly used for highly thermomechanically loaded blades of aircraft gas turbine engines. The APS process (Ref 10, 11) meanwhile displays often operational robustness comparable to EB-PVD and improved economic viability; hence, more TBCs are now being developed based on this process. Typically, static components, such as combustor cans and vane platforms, are coated by APS. In stationary gas turbines, blades are also frequently coated by thermal-spray processes (Ref 12).

In thermally sprayed coatings, splats are separated by interlamellar pores resulting from rapid solidification, very

Georg Mauer, Maria Ophelia Jarligo, Daniel Emil Mack, and **Robert Vaßen**, Institut für Energie- und Klimaforschung (IEK-1), Forschungszentrum Jülich GmbH, Jülich, Germany. Contact e-mail: g.mauer@fz-juelich.de.

fine voids formed by incomplete intersplat contact or around nonmolten particles, and cracks due to thermal stresses, and tensile quenching stress (Ref 13). Such porosity is a key characteristic of modern thermally sprayed ceramic TBCs. In particular, the heat flux transfer to the metallic bondcoat and component is reduced by evenly spaced porosity (Ref 14). Moreover, the more porous the coating microstructure is the more scattering centers are introduced into it. In this way, the radiative heat load deposited onto the gas turbine components is also reduced (Ref 15). To achieve specific porosities, the melting status of the powder particles plays a key role which can be controlled on the basis of in-flight particle temperature measurements (Ref 16). Typical porosities for TBC topcoats are 15% by volume and higher. Moreover, segmentation cracks can increase the strain tolerance of TBCs resulting in a reasonable thermal shock resistivity (Ref 17).

Partially yttria-stabilized zirconia (YSZ) with yttria contents ranging from 6 to 8 wt.% is frequently used as TBC material because of its high thermal expansion coefficient (TEC) and its relatively good fracture toughness. YSZ as formed by the APS or EB-PVD process consists of the metastable t'-phase. On prolonged exposure at elevated temperatures, it decomposes into high-yttria and low-yttria phases. The latter transforms on cooling into the monoclinic phase with an associated large volume increase, which may result in the catastrophic failure of the TBC (Ref 18). The accepted upper limit for long-term use is 1200 °C. In addition to the limited phase stability, sintering coarsens the pores and reduces the high-temperature capability as it leads to an increase of thermal conductivity and a loss of strain tolerance of the coatings and hence early failure (Ref 19).

To overcome these shortcomings of YSZ-based TBCs, alternative materials with higher-temperature capabilities are under investigation (Ref 12). Interesting candidates are those materials with pyrochlore (e.g., $La_2Zr_2O_7$, $Gd_2Zr_2O_7$), spinel ($MgAl_2O_4$), perovskite (e.g., $SrZrO_3$), or magnetoplumbite (e.g., $LaLiAl_{11}O_{19}$) structures with high melting points (Ref 20, 21). In particular, more complex perovskite forms such as $Ba(Mg_{1/3}Ta_{2/3})O_3$ and $La(Al_{1/4}Mg_{1/2}T_{1/4})O_3$ have promising bulk properties for TBC applications. However, the TECs of these new materials are still lower than those of substrates and bondcoats, leading to thermal stresses in the TBC system. Moreover, relatively low toughness values are observed. As a result, the thermal cycling properties are poorer than those of YSZ coatings. One way for the remediation of this shortcoming is to use layered topcoats. Failure of TBC systems often occurs in the TBC close to the bondcoat/topcoat interface. At this location, YSZ is used as a TBC material with a relatively high TEC and high toughness (Ref 22, 23).

In this study, recent research activities on the responses of new TBC materials to the complex demands of modern gas turbine applications are reviewed. Figure 1 visualizes that material design is a coordinated result from materials science on the one hand, and processing development on the other hand. Thus, successful solutions require competences in both these fields as well as knowledge on the application-specific issues. This context is the basis for the research study on TBCs in the Institute of Energy and Climate Research (IEK-1) at Forschungszentrum Jülich, Germany. Also new thermal-spray processes are developed here, namely, the suspension plasma spraying (SPS) and plasma spraying-physical vapor deposition (PS-PVD). However, this article is confined to ceramic TBC coating systems manufactured by APS with particular emphasis on process-related solutions by employing diagnostic tools. New processing methods as well as bondcoat developments are part of other publications (Ref 24-26).

2. Pyrochlores

2.1 Lanthanum Zirconate

Several zirconate pyrochlores show low thermal conductivities as well as high thermal stabilities. Among them, lanthanum zirconate $La_2Zr_2O_7$ (LZ) is phase stable to its melting point as it can largely tolerate vacancies at the La^{3+}, Zr^{4+}, and O^{2-} sites. At the same time, it displays a lower thermal conductivity (1.56 Wm^{-1} K^{-1}, bulk material) and a lower sintering tendency when compared with YSZ. As mentioned before, pyrochlores are applied in combination with YSZ in double-layer TBC systems.

The $La_2O_3{\cdot}ZrO_2$ phase diagram shows a stable pyrochlore region up to the melting temperature of 2295 ± 10 °C and the stability region ranges from approximately 33 to 35 mol.% La_2O_3 at 1500 °C (Ref 27). Below the melting

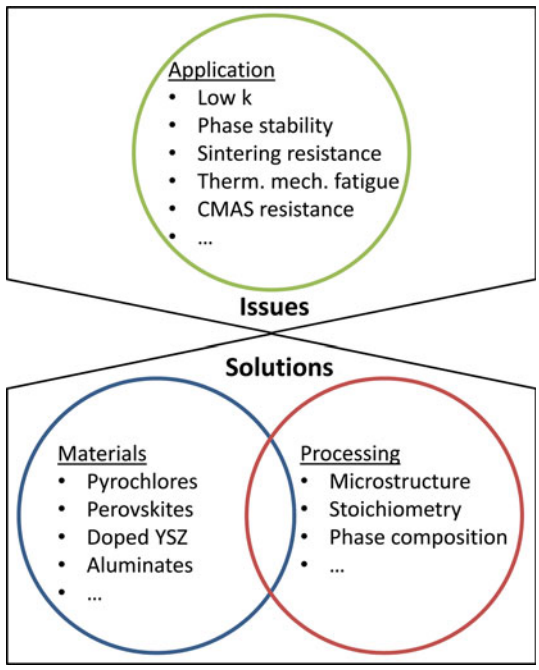

Fig. 1 The context of application-specific issues, materials science, and processing development as the basis to acquire TBC solutions meeting the complex requirements of modern gas turbines

temperature, no fluorite phase occurs since solidification starts directly in the form of pyrochlore. However, considerable amounts of metastable fluorite phase are formed in the case of rapid solidification, which is typical of plasma-spray conditions. Such fluorite phase is transformed to pyrochlore at temperatures above 1000 °C (Ref 28, 29). This is not critical as such transformation is not associated with significant volume change.

The processing of LZ by atmospheric plasma spraying is challenging because La_2O_3 is prone to evaporate in the plasma plume resulting in non-stoichiometric coatings (Ref 27). This might be detrimental for TBC performance as thermophysical properties are affected (Ref 30, 31). Similar problems are known to emanate from EB-PVD LZ coatings (Ref 32). La_2O_3 shows considerably higher vapor pressure when compared with ZrO_2 (Ref 33). Although reference data from the literature are not in good agreement, it is evident that the vapor pressure of lanthania is at least one magnitude higher than that of zirconia.

In a recent study (Ref 34), atmospheric plasma spray (APS) experiments were performed with a TriplexPro™-200 plasma torch (Sulzer Metco, Wohlen, Switzerland) at different power levels between 15 and 51 kW to adjust different degrees of evaporation and thus stoichiometry. For this, the current was varied between 200 and 525 A while the plasma gas flow was 46 slpm Ar + 4 slpm He and the spray distance was 90 mm. Figure 2 shows the lanthania contents determined by chemical analysis versus torch input power between 15 and 51 kW. The feedstock powder showed an almost stoichiometric composition. The lanthania content in the sprayed LZ coatings already exhibits a small initial drop at low torch input power down to 32.9 mol.% (La/Zr atomic ratio of 0.99) and if the power is raised, then it continues to decrease to 27.0 mol.% at 51 kW corresponding to a La/Zr atomic ratio of 0.75. Here, up to 24.8% of the lanthanum content in the powder feedstock was lost.

X-ray diffraction (XRD) analyses of the LZ coatings revealed that the content of the defective fluorite phase grows as the torch input power is raised. Furthermore, with increasing torch input power, the XRD peaks shift to larger 2θ values indicating the increasing non-stoichiometry.

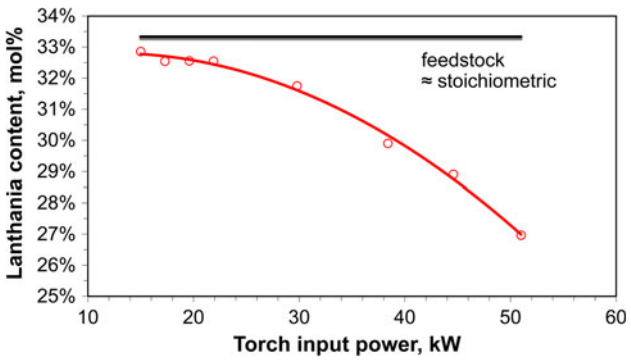

Fig. 2 Lanthania contents determined by chemical analysis vs. torch input power between 15 and 51 kW (Ref 34)

The lattice parameters were found to be directly correlated to the stoichiometry (Ref 34). At 30 kW and above, the fluorite phase content is 90 wt.% or more. In each case, the balance is pyrochlore phase. Obviously, the formation of the defective fluorite phase, which is less ordered than the pyrochlore phase, is an effect of the rapid cooling upon impingement on the substrate of such material fractions which are still molten at that time. In contrast, the material fractions which have already solidified during flight may be deposited as pyrochlore.

Quantitative energy dispersive spectroscopy (EDS) point analyses of the coatings sprayed at the highest torch power of 51 kW confirmed the existence of areas with considerable lanthanum depletion resulting in large amounts of zirconia along with the lanthanum zirconate. Very low La/Zr atomic ratios down to 0.28 were found corresponding to zirconia contents of up to 82 mol.% with only 18 mol.% lanthanum zirconate. Consequently, significant amounts of metastable cubic zirconia can develop. This was confirmed by phase analysis of annealed coatings sprayed at low and high torch powers. During annealing for 4 h at 1400 °C, the fluorite transformed to pyrochlore phase and, in particular, the sample sprayed at high torch power developed monoclinic and metastable zirconia phases which transform and undergo specific volume changes during thermal cycling leading to early failure.

In-flight particle characteristics were measured by the DPV-2000 (TECNAR, St-Bruno, QC, Canada) diagnostic system (Ref 35). The particle temperature distributions for the lower range of torch input power show multimodal shapes, as shown in Fig. 3. Hence, the distributions were fitted with Gaussian functions to identify different particle fractions. The first two peaks at constant and almost constant temperature, respectively, are assumed to be associated with solidification (or the powder melting temperature) and release of fusion enthalpy. Details can be found elsewhere (Ref 34). Hence, particle diagnostics proved to be an effective tool to determine the melting degree. Based on such an analysis, spray parameters can be identified ensuring minimal lanthania evaporation, and at the same time, suitable microstructures and deposition efficiencies.

2.2 Gadolinium Zirconate

Currently, one of the most promising resistant materials against high-temperature corrosion of CMAS is gadolinium zirconate, $Gd_2Zr_2O_7$. This material has been found to play an important role in damage mitigation of TBCs in aircraft engines (Ref 5). CMAS glass penetrating the conventional YSZ-TBC forms a stiff glaze on cooling, which results in the reduction of strain tolerance of the coatings during thermal cycles (Ref 5, 36). However, in the case of gadolinium zirconate, upon infiltration of CMAS melt, an impervious reaction zone composed of complex anorthite, appatite, and calcium zirconate phases is formed in the region where CMAS infiltration stops (Ref 37, 38).

Since, gadolinium zirconate is very costly, a composite coating with YSZ can have additional benefits of

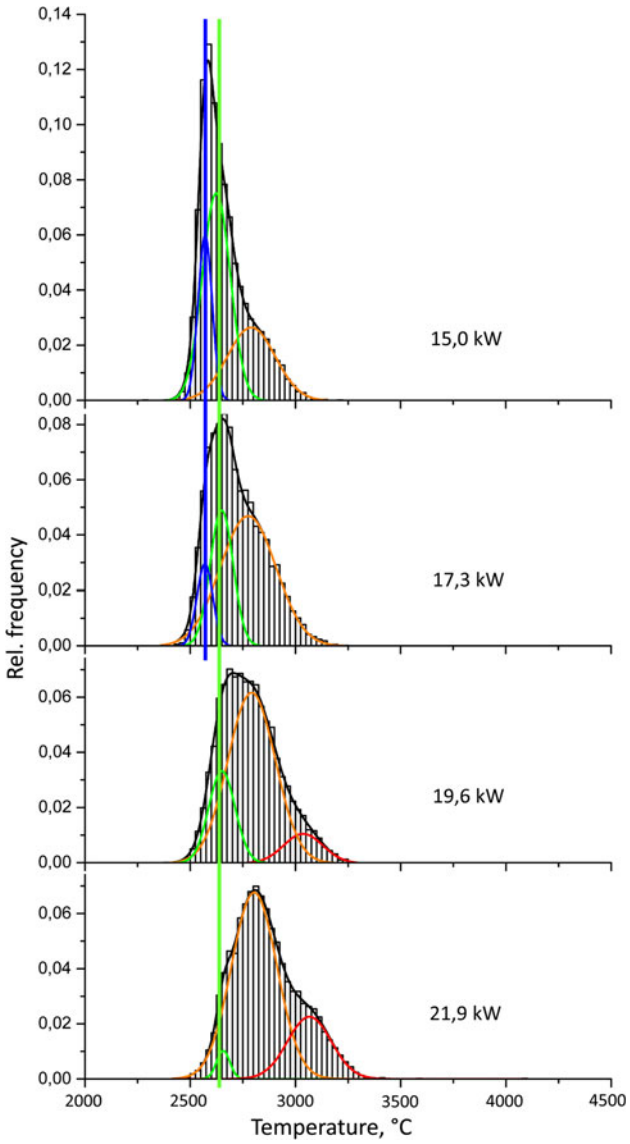

Fig. 3 LZ particle temperature distributions as estimated using two-color pyrometry for the lower range of torch input power between 15.0 and 21.9 kW (Ref 34)

durability and affordability (Ref 39). To deposit coatings by APS, such a powder mixture is, however, challenged by the different melting characteristics of the particles. With TriplexPro™ (Sulzer Metco, Wohlen, Switzerland) and Ar/He plasma gas flow of 46/4 slpm, an electric arc current of 500 A is typically required to deposit YSZ, while a maximum of only 350 A is needed for gadolinium zirconate to achieve minimalistic decomposition of Gd_2O_3 during spraying. As shown in Fig. 4, although the difference in their melting temperature is quite small, gadolinium zirconate has a large number of particles with very high temperatures as compared with YSZ. This could be attributed to the higher heat capacity of YSZ as compared with most pyrochlores (Ref 20). Spray parameters for the TriplexPro™ torch were carefully optimized to achieve a compatible set of parameters for the composite mixture. The 350 A current was adopted with 50/4 slpm Ar/He plasma gas flow. The resulting as-sprayed coating for 1:1 YSZ-GZO is shown in Fig. 5(a). About 16% porosity was detected by mercury intrusion. Corrosion resistance test was conducted isothermally in an oven at 1400 °C for 5 h using a CMAS corrosion agent with additional high Fe-composition. The reaction products and microstructure were evaluated using XRD and scanning electron microscope (SEM). Figure 5(b) shows that only up to 30% of the total coating thickness is infiltrated with CMAS after 2 h and a reaction zone has been formed. Iron-rich phases crystallize on the surface of the coating. Therefore, the presented method of producing GZO-YSZ composite coatings could certainly work regardless of whether non-stoichiometric gadolinium zirconate phases are deposited together with YSZ.

3. Perovskites

The perovskites with structural formula ABO_3 are characterized by high melting points, low thermal conductivities, and high TECs. Additionally, they offer the possibility of extensive substitution of ions at the *A* or/and *B* site, which enables the properties of the materials to be selectively influenced (Ref 40).

3.1 Complex Perovskites $Ba(Mg_{1/3}Ta_{2/3})O_3$ and $La(Al_{1/4}Mg_{1/2}T_{1/4})O_3$

The most promising candidates for advanced TBC materials development are those with high melting temperatures in addition to phase stability and low thermal conductivity in general. Among these materials, complex perovskite with $Ba(Mg_{1/3}Ta_{2/3})O_3$ (BMT) composition has melting temperature of ~3000 °C and is considered among the most refractory oxides ever known to science (Ref 41, 42). Another material candidate from this system is $La(Al_{1/4}Mg_{1/2}T_{1/4})O_3$ (LAMT). It can accommodate three cations in the *B*-site and has lower thermal conductivity than BMT. The bulk properties include low values of thermal conductivity (~2 $Wm^{-1}\ K^{-1}$) and high coefficient of thermal expansion (~11 × $10^{-6}\ K^{-1}$) similar to YSZ making it very promising for TBC applications (Ref 43, 44).

APS of these perovskite materials is often challenged by the formation of secondary phases which are deficient in Mg (indicated by white arrows in Fig. 6). These phases are more pronounced after annealing at 1200 °C (Ref 45-47). Their presence caused an integral effect on the low thermal cycling lifetime of the coatings because of the differences in their thermal properties. To avoid deposition of inhomogeneous coatings, in-flight particle diagnostics during APS were focused on preventing the formation of secondary phases during plasma spraying (Ref 48).

Different process maps were generated to investigate the influence of plasma parameters to the deposited phases. A process map for LAMT obtained by spraying with

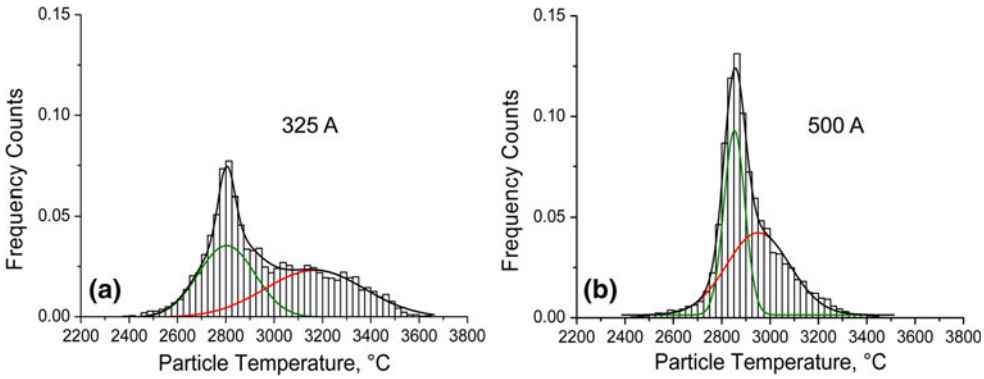

Fig. 4 In-flight temperature profiles of gadolinium zirconate (a) and YSZ (b). The temperature at the 1st maxima is presumed to be the melting temperature of the powders

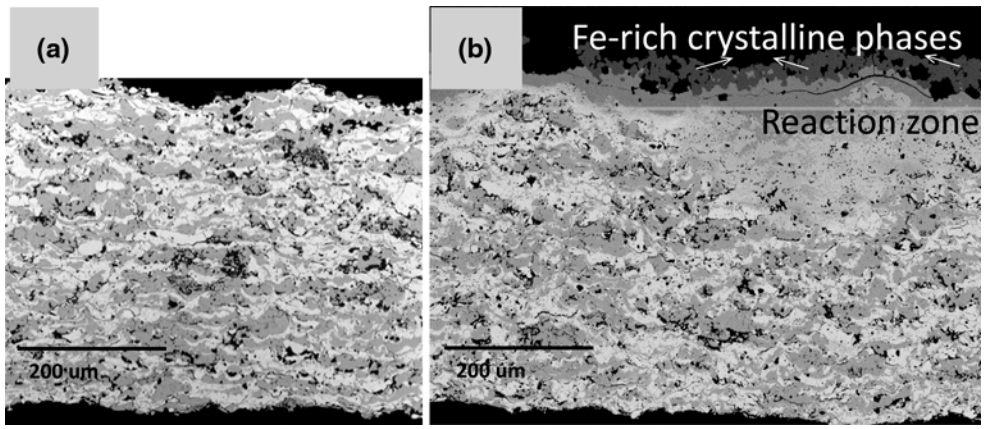

Fig. 5 Cross section of as-sprayed 1:1 gadolinium zirconate-YSZ composite coating (a) and the coating infiltrated with high-iron CMAS at 1400 °C (b). The white layers belong to gadolinium zirconate while the gray shades are made of YSZ

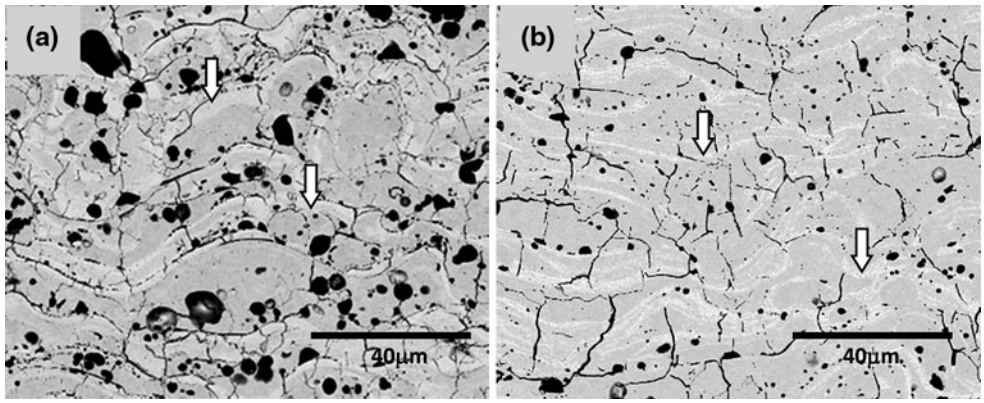

Fig. 6 SEM micrographs of plasma-sprayed (a) BMT and (b) LAMT coatings after annealing at 1200 °C for 3 h (Ref 48)

the Triplex II gun (Sulzer Metco, Wohlen, Switzerland) suggests that at 40/4 slpm Ar/He gas flow rate, 550 A of gun current and increasing spray distance until an optimum value of 200 mm, the particle temperature increases as the particle decelerates in the plasma plume (Ref 48).

The residence time of the particles in the plasma plume was also found to strongly influence the decomposition of the component phases (Ref 48). This was proven by investigating the composition of the particles during flight by spraying into water. This technique was adopted to capture the component phases during particle flight. A composition with excess Mg was used as powder feedstock. Spherical particles collected from spraying into water using the parameter set mentioned above show that

some dark spots which are Mg rich are found on the surface of the particles. Among the oxide components of BMT and LAMT, MgO has the highest vapor pressure and is therefore more prone to decompose (Ref 49). As the particles are heated up during spraying, Mg diffuses to the surface prior to vaporization. Owing to rapid cooling upon spraying into water, some of the Mg atoms from incompletely molten large particles are not able to volatilize and re-solidify with other phases on the surface of the particles. Increasing decomposition of Mg was also reported with increasing amount of electric arc current (Ref 44, 48, 50).

Apart from particle diagnostics, analyses of single splats were also conducted for the complex perovskites. With higher torch power, the splats are more fingered as shown in Fig. 7 indicating that the particles have very low viscosity upon landing. At lower power, the BMT splat is more cracked, while the LAMT is more of a pancake which is characteristic for solidified amorphous phases (Ref 48).

The lifetime of the coatings were found to improve significantly with the application of reduced power of either Triplex II or TriplexPro torch as shown in Fig. 8 (Ref 51). The complex perovskite coatings had minimal secondary phases present and were tested in double-layer systems with YSZ as sub-layer.

3.2 Strontium Zirconate and the Gd- and Yb-Doped Systems

Strontium zirconate $SrZrO_3$ is another promising perovskite material for TBC application due to its high melting point (2610 °C) and high TEC (~11 × 10^{-6} K^{-1}) (Ref 20, 43). During plasma spraying, SrO having a higher intrinsic vapor pressure was found to volatilize faster than ZrO_2 resulting to the deviation of stoichiometric composition in the deposited coating (Ref 52). The existence of excess ZrO_2 in the plasma-sprayed $SrZrO_3$ coating might also influence the coating properties. Quantitative investigation of the partial evaporation of $SrZrO_3$ by spraying powders into water was therefore conducted (Ref 53). Some new needle-like structures were collected from the water container and they contain only Sr (Fig. 9). These are probably condensates of Sr during plasma spraying.

Once the initial composition of the powders was fixed, the final Sr/Zr ratio of the sprayed coating was determined by the spraying current, distance and particle size of the starting powders. Particle diagnostics using Accuraspray-g3 (TECNAR, St-Bruno, QC, Canada) revealed that increasing spray current lead to higher particle temperature and higher evaporation of Sr (Ref 53). Similar behavior was also observed when the spray distance was increased. This evaporation can also be effectively reduced by effectively increasing the particle size of the starting feedstock (Ref 44, 50, 53). When traces of $SrCO_3$ and metastable tetragonal ZrO_2 can be detected in the as-sprayed coating, during sintering, $SrCO_3$ reacts with part of ZrO_2 to form $SrZrO_3$ again and the remaining metastable tetragonal ZrO_2 transformed into monoclinic ZrO_2 (m). After sintering, pure $SrZrO_3$ coating can be produced only when the Sr/Zr ratio of the coating is a little larger than unity.

An attempt to improve the thermophysical properties of $SrZrO_3$ by doping with Gd and Yb, was also conducted (Ref 43).The results of specific heat capacity and thermal conductivity measurements reveal that doping Yb_2O_3 is more effective in reducing the specific heat capacity and thermal conductivity of $SrZrO_3$ than doping with Gd_2O_3. The Young's moduli of the modified $SrZrO_3$ were found to be lower than that of YSZ, which might yield higher strain tolerance for coatings. Furthermore, comparing the thermal cycling lifetime of the single-layer and the double-layer systems, the latter have much longer thermal cycling lifetimes at a surface temperature of 1250 °C, which are comparable to that of the YSZ coating at similar surface temperature. In particular, a major advantage for $Sr(Zr_{0.9}Yb_{0.1})O_{2.95}$/YSZ double-layer system is that its thermal cycling lifetime is better compared to that of the optimized single-layer YSZ topcoat at a surface temperature of 1350 °C. This could be a good alternative for single-layer YSZ coating at higher temperature applications (Ref 43).

4. Aluminates

Materials from some aluminate systems as yttrium aluminium garnet (YAG) or rare earth (RE) hexaaluminates are promising TBC candidates for use at surface temperatures exceeding 1300 °C due to their high melting point, high thermal expansion, low thermal conductivity, excellent longtime sintering resistance, and structural stability (Ref 54). As mentioned above, increased resistance against glassy deposits can also be expected because of the inherent Al content of those materials (Ref 5). Previous results not reported here indicate the validity of this expectation.

From the practical point of view of plasma-spray processing, a special feature of those materials is their tendency to be deposited in partly amorphous state during thermal-spray processing. Upon subsequent annealing, e.g., during operation, rapid recrystallization occurs which is coupled with reduction of bulk volume (Ref 54, 55). This causes a microstructure with cracks on the meso-scale which offers potentially advantageous thermal shock properties (Ref 56). Depending on the deposition parameters and subsequent heat treatment, a network of segmentation cracks is formed. The microstructure is similar to that found in flexible sandstone (Ref 57) and can be assumed to support improved strain tolerance.

An example of the influence of processing parameters is given here on the hexaaluminate type of $LaLiAl_{11}O_{18.5}$ with magnetoplumbite structure which shows extraordinary pronounced shrinkage and segmentation crack formation. Figure 10 shows micrographs from two free standing coatings in the as-sprayed condition which have been manufactured from the same feedstock with a Sulzer Triplex II gun by distinctly different thermal spray parameters. Parameters and some properties are summarized

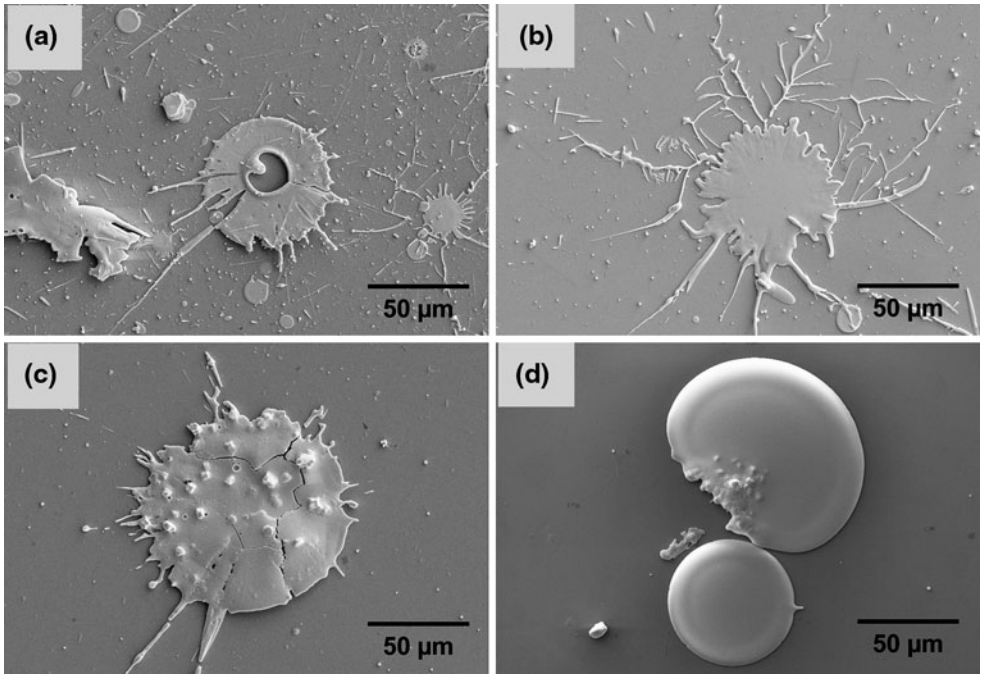

Fig. 7 Single splats of BMT (a, c) and LAMT (b, d) deposited using applied power of 49 kW (top) and 25 kW (bottom)

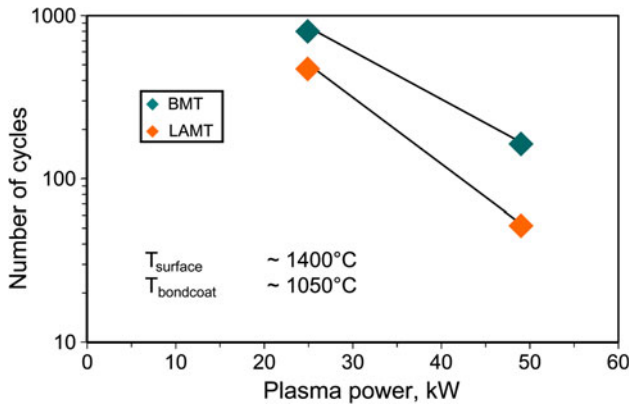

Fig. 8 Lifetime trends of thermal barrier coatings from double-layer systems of complex perovskite and yttria-stabilized zirconia

in Table 1. The first coating, having an initial porosity of 14% (named ''porous''), has been sprayed with relatively lower power and shorter distance to the target compared with the second one, having an initial porosity of 8% (named ''dense'').

Achieving lower porosities by means of increasing the gun power is not unusual in plasma spraying because of the typically associated higher degree of melting and the higher particle velocity. Nevertheless, in the given example a more thorough analysis of the spraying process by means of DPV 2000 reveals that relative values of the average particle temperature and velocity are reversely proportional to the trend expected from porosity results. As can be seen from the upper part of Fig. 11, for an arc current of 450 A, the spread and the average of particle temperatures is decreasing with increasing distance. This indicates that melting of the particles presumably occurs already at low distances within the plasma plume and particles are allowed to cool down and slow down before impact. The temperature distribution of particles sprayed with the ''dense'' parameter set of the given example is shown in the lower part of Fig. 11 thereby clarifying that the influence of the increased distance overbalances the increased gun power regarding temperatures and velocities.

Considering the material feature of amorphous quenching and the apparent downward shift of temperature for the ''solidifying particle'' fraction with distance from Fig. 11, the deposition behavior of the hexaaluminate can be rather interpreted by assuming solidification and crystallization of potentially undercooled melts as it has been similarly discussed for YAG (Ref 55). The larger heat carried with the particles on impact for conditions ''porous'' might allow for a larger degree of re-crystallization compared with potentially undercooled particles of condition ''dense''. The local volume shrinkage accompanied with splat-wise re-crystallization can be correlated with the increased porosity as found. This interpretation is also supported by observations of higher crystallinity in the XRD characterization and lower residual shrinkage on macroscopic crystallization treatment in the case of the ''porous'' coating. Further important parameters influencing the controlled crystalline deposition for these kinds of materials are specially substrate temperature and particle size, both influencing the degree of melting and the kinetics of re-solidification.

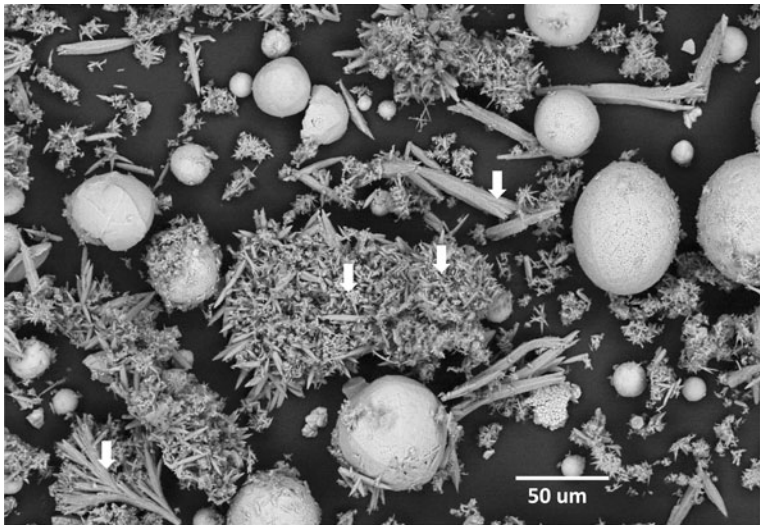

Fig. 9 Plasma-sprayed SrZrO particles collected from water

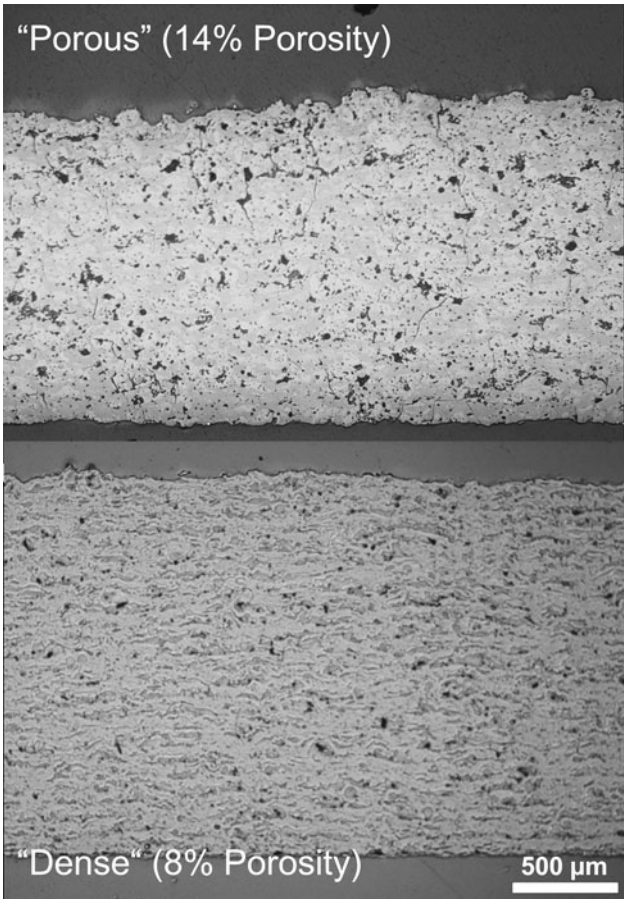

Fig. 10 Optical micrographs of $LaLiAl_{11}O_{18.5}$ hexaaluminate coatings manufactured with parameters as summarized in Table 1

Table 1 Selected processing parameters and coating properties for $LaLiAl_{11}O_{18.5}$ hexaaluminate coatings

	Porous	Dense
Ar/He-flow	50/4 slpm	50/4 slpm
Current	450 A	520 A
Spray distance	100 mm	200 mm
Feed rate	15%	20%
Avg. particle temp.	2740 °C	2590 °C
Avg. particle velocity	280 m/s	240 m/s
Porosity	14%	8%
One-dim. shrinkage	~1%	~2.5%

slpm, standard liters per minute

5. Doped YSZ

5.1 YSZ Doped by TiO_2

A recent study has found that substitution of up to ~15 mol.% TiO_2 for ZrO_2 into the single-phase tetragonal (t') 7-8 wt.% YSZ increases toughness and diminishes the transformation phenomenon even up to 1600 °C (Ref 58). This offers a unique opportunity to enhance the performance of the standard YSZ-based TBCs. To develop an improved YSZ-TBC system based on the addition of titania, a better understanding of the process parameters is necessary. Other than particle diagnostics using two-color pyrometry, the surface roughness of the plasma-sprayed single splats have also been reported to provide information on the status of molten and solidifying particles as they are deposited to form into splats (Ref 59). Figure 12 shows the morphology of a partly molten splat and its corresponding three-dimensional surface profile with exaggerated height obtained by a white light profilometer

(LT-9000 confocal laser microscope, Keyence, Neu-Isenburg, Germany). Surface roughness was determined using the international measurement standard ISO 4287. The R_z values were determined from the differences of the height and depth of the splat topography to a median height. The values were then averaged for every material composition for the overall surface roughness of the deposited single splats. The thickness or roughness of the formed splat suggests the degree of particle melting. Rougher splats are formed from solidified particles which are probably slightly molten upon impact while thin splats are formed from flattening of majorly molten particles as they impact the substrate. Table 2 shows a summary of the average roughness of YSZ splats with varying amount of titania. The values obtained suggest that there is no direct relationship between TiO_2-doping and the overall surface roughness of the deposited single splats. Therefore, doping with up to 15 mol.% of titania does not significantly alter the melting characteristics and coating microstructure of pure YSZ.

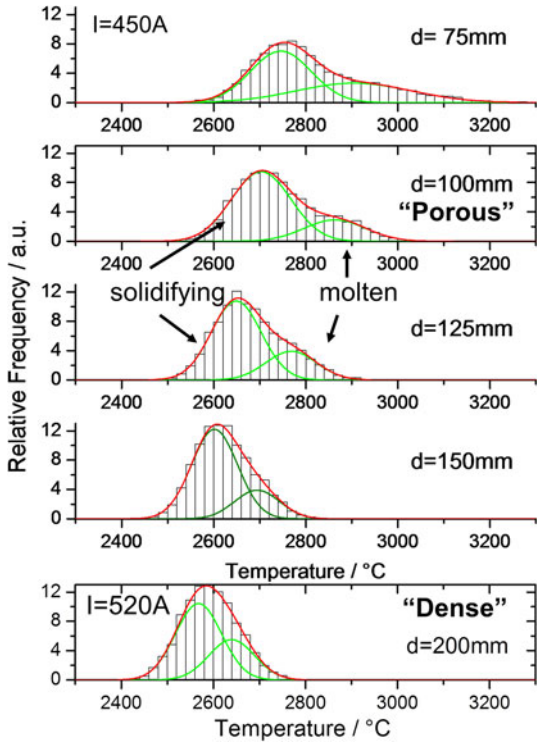

Fig. 11 $LaLiAl_{11}O_{18.5}$ hexaaluminate particle temperature distributions as estimated using two-color pyrometry depending on stand-off distance at arc current 450 A (upper part) and for deposition condition ''dense'' (lower part)

The lamellae formed from the flattening of plasma-sprayed feedstock have a heterogeneous microstructure composed of randomly distributed pores, micro-cracks and unmolten particles (Ref 59). The mercury porosity measurement conducted on the coatings reveal that at gun current of 500 A (TriplexPro™), plasma gas flow of 46/4 slpm Ar/He, the total average porosities of the coatings are nearly the same as shown in Fig. 13. The increased addition of titania has no direct influence on the porosity of the coating with varying gun current supply. However, as the applied gun current increases, the porosity of the coatings decreases. This is consistent with the observations in the particle temperature distribution reported in Ref 48 where increasing gun current results in increasing amount of molten particles that lead to the deposition of coatings with decreased porosity. The coating lamellae are formed from increasing amount of molten particles of low viscosity with increasing gun current. The influence therefore is not chemical but rather process controlled. In this case, it would be erroneous to assume that since higher Ti induces melting, then denser coatings should be produced. As revealed in the surface roughness and porosity measurements, titania doping does not have a significant influence on the coating microstructure. Also, on plasma spraying, particles may fragment as they exit the plasma injector causing the smaller-sized particles to flow along the plasma fringes and not into the main spray stream. These particles are deposited into the coatings as

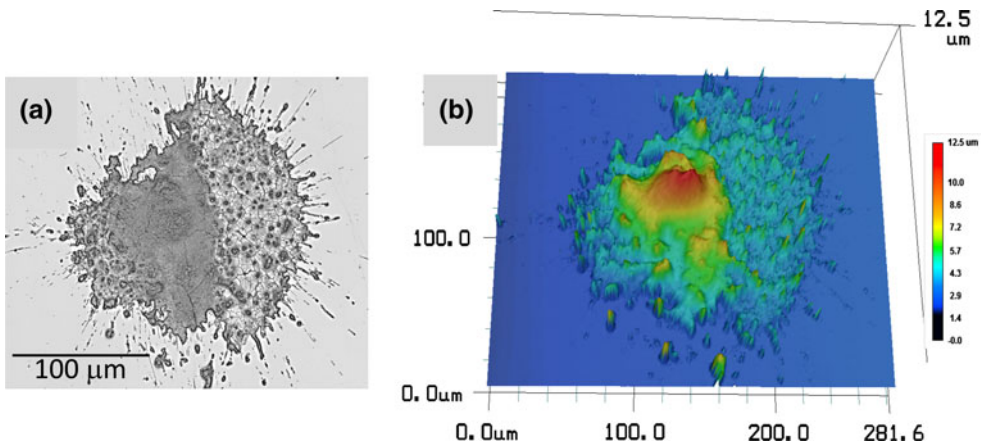

Fig. 12 Single splat (a) morphology and (b) corresponding exaggerated 3D surface profile of Ti-doped YSZ obtained by a white light profilometer

unmolten particles that may significantly contribute to the increased amount of micropores which are also included during porosity measurements. As the results suggest, the addition of titania does not significantly influence such a process phenomenon.

Table 2 Average surface roughness of single splats from YSZ powders with different doping amounts of TiO_2

TiO_2 (mol.%)	Rz (μm)±
0	62 ± 19
7.6	69 ± 21
15.2	62 ± 15

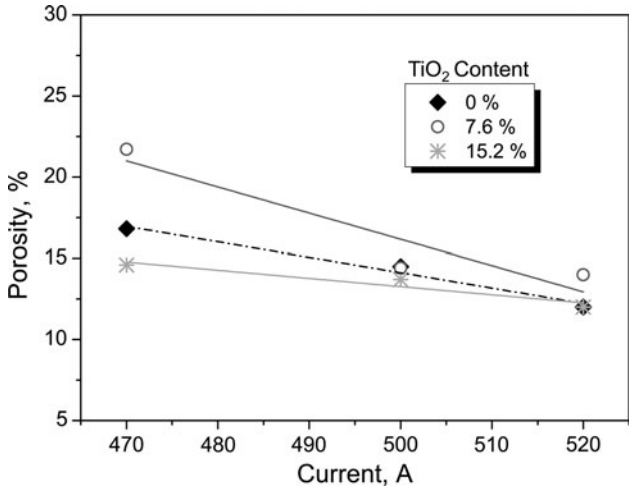

Fig. 13 Porosity values as a function of gun current for the different Ti-substituted coating compositions

Up to now, the phase diagrams of the ternary ZrO_2-TiO_2-$YO_{1.5}$ systems above 1300 °C are still unknown. Derivations from correlated experimental and mathematical investigations reveal that on increasing the temperature from 1300 to 1600 °C, the stability region of the pyrochlore phase widens as more Ti is accommodated (Ref 60). The maximum solubility of yttria and titania into the tetragonal zirconia at 1300 °C was also reported to be limited to approximately 6 and 12 mol.%, respectively. Mathematical calculations on experimental data and phase analyses derived from slow heating and cooling experiments, predicted considerably varying phase boundaries at higher temperature values for the ternary systems. The composition therefore with 15.2 mol.% TiO_2 is vulnerable to the formation of brittle Ti-rich pyrochlore phases during spraying where plasma temperature reaches extremely high values. This phenomenon is clearly manifested in the microstructure profile of the thermally cycled samples at 1400 °C (Ref 61). Although the as-sprayed coatings have slightly increased in tetragonality with increasing amount of titania, the lifetime of the coatings is not influenced by the doping of titania at the investigated composition range. The tips of the cracks of the cycled samples are rich in Ti and this is more pronounced for samples with higher amount of Ti-dopant as shown in Fig. 14. This would imply that coating embrittlement is induced by the formation of pyrochlore phases. It is therefore recommended to dope yttrium-stabilized zirconia with lower percentages of TiO_2 than the investigated compositions of 7.5-15 mol.%.

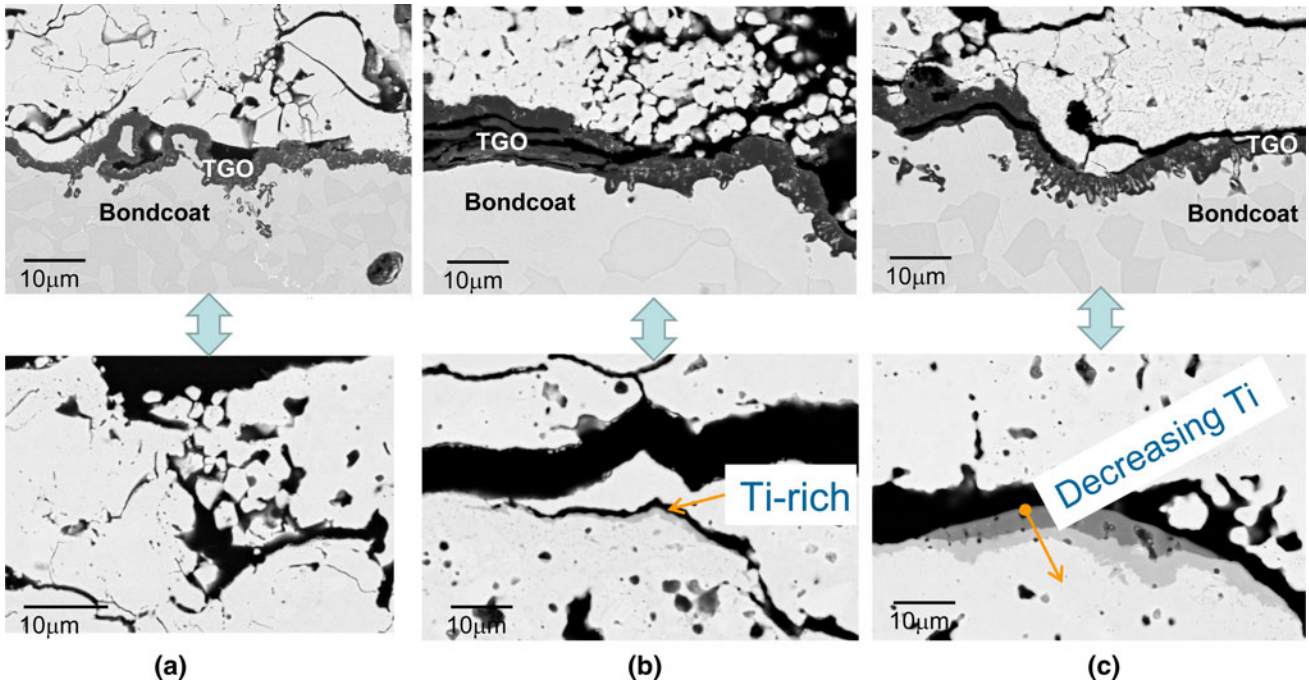

Fig. 14 Cross-sectional images of thermally cycled samples at 1400 °C. Undoped YSZ is (a), while (b) and (c) are doped with 7.6 and 15 mol.% of TiO_2, respectively

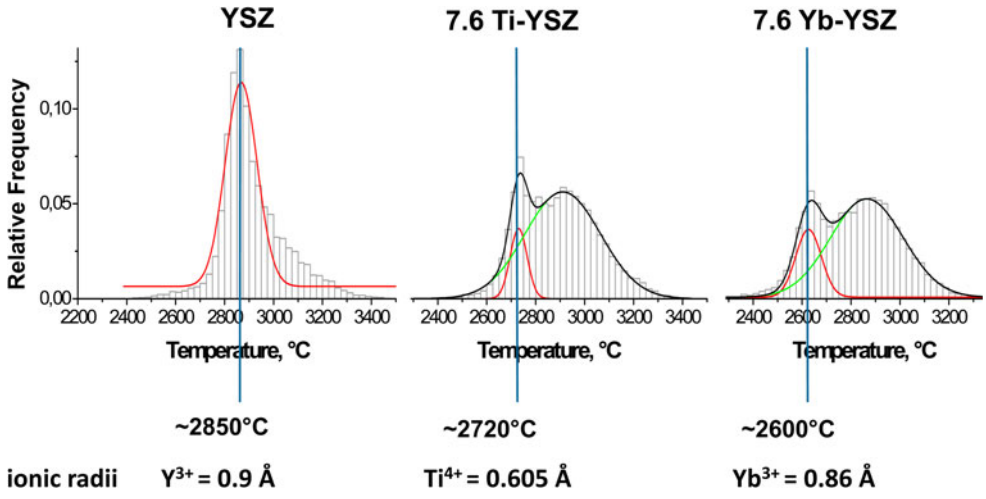

Fig. 15 Particle temperature profiles for Ti^{4+}- and Yb^{2+}-doped YSZ coatings

Table 3 Summary on strengths and limitations of new TBC materials under review

Materials	Strengths	Limitations
Pyrochlores		
$La_2Zr_2O_7$*	High temperature capability High thermal expansion coefficient	Highly prone to decomposition during plasma spraying
$Gd_2Zr_2O_7$*	Good resistance to CMAS attack Cost-effective applicability in composite with YSZ	Prone to decomposition during plasma spraying
Perovskites		
$BaMg_{1/3}Ta_{2/3}O_3$*	High thermal expansion coefficient at 1473 °C	Prone to Mg evaporation during plasma spraying Low fracture toughness
$LaAl_{1/4}Mg_{1/2}Ta_{1/4}O_3$*	Good resistance to CMAS attack	Prone to Mg evaporation during plasma spraying
(Gd,Yb)$SrZrO_3$*	Good resistance to thermo-mechanical fatigue	Prone to Sr evaporation during plasma spraying
Hexa-aluminate		
$LaLiAl_{11}O_{18.5}$*	Good resistance to CMAS attack Good resistance to thermo-mechanical fatigue	Potential recrystallization needs to be considered to ensure desirable microstructure Higher thermal conductivity than YSZ
Doped YSZ		
TiO_2-YSZ	Promising material for resisting CMAS attack High fracture toughness for TiO_2 <5 mol.%	Prone to phase transformation with Ti-dopant higher than 5 mol.%
Yb_2O_3-YSZ	Good resistance to thermo-mechanical fatigue	Until now, only 7.5 mol.% Yb_2O_3 has been investigated

*Double-layer systems

5.2 YSZ Doped by Yb_2O_3

Ytterbium cation (Yb^{3+}) doped into the YSZ structure in similar manner as doping with Ti, was found to improve the thermomechanical properties and particularly lower the thermal conductivity of the state-of-the-art TBC (Ref 62). Ytterbium cation has smaller ionic radius compared with Ti^{4+}. Characteristics of YSZ powder compositions doped with Yb and Ti were compared during plasma spraying. Feedstock powders were sprayed with Triplex-Pro™ plasma torch with current of 500 A and Ar/He gas flow of 50/4 slpm and spray distance of 200 mm. The particle temperature profiles and corresponding ionic radii of dopant cation are plotted in Fig. 15 (Ref 63). Results show that the Yb-doped YSZ has the lowest melting temperature (as indicated by the temperature at the first maxima which is assumed to be the powder melting temperature) compared with the undoped and Ti-doped YSZ. This implies that Yb cation dopant, with larger ionic radius has the higher tendency to decrease the melting temperature of YSZ ceramics during plasma spraying. With the same spray parameters, the porosity of the Yb-YSZ coating is about 15% which is also much lower than that of the Ti- and undoped YSZ coatings with porosity values above 20%. When the thermal cycling lifetime was obtained at 1400 °C surface temperature in a gradient burner rig test, the Yb-doped YSZ with the lowest porosity has the lowest lifetime compared with the other compositions. However, the performance of the Yb-doped coating can be improved by adjusting spray parameters like decreasing the plasma power to obtain higher coating porosity, thus obtain lower heat conduction through the coating during thermal cycles.

6. Conclusion and Outlook

In this study, recent research activities on responses of new TBC materials to the complex demands of modern gas turbine applications are reviewed. Such alternative materials with higher-temperature capabilities are those with pyrochlore, perovskite, or magnetoplumbite structures. However, their processing by thermal spraying often turns out to be challenging. The more complex the composition is, the more different is the stability and volatility of the constituents. Thus, stoichiometry of the deposited coatings can change and undesired secondary phases may be formed. Furthermore, the coating microstructure is affected if the melting behavior and thermal properties of the constituents differ. In addition, combining proper optimization of spray process parameters and selection of promising dopant cations, the existing superior properties of the zirconia-based TBCs can be well improved. Table 3 shows a summary of strengths and limitations of the reviewed new TBC materials reported in this manuscript.

The examples discussed in the present article reveal that material design needs coordinated efforts on materials science on the one hand and processing development on the other hand. In this context, process diagnostics were found to be valuable tools.

Acknowledgments

The authors are grateful to Dr. Jürgen Malzbender (IEK-2), Mr. Mirko Ziegner (IEK-2), Mrs. Hannelore Lippert (ZCH), and the colleagues of IEK-1 in Forschungszentrum Jülich GmbH for their help in carrying out the experiments which results are reported in this article.

References

1. R.A. Miller, Current Status of Thermal Barrier Coatings—An Overview, *Surf. Coat. Technol.*, 1987, **30**, p 1-11
2. R. Vaßen, H. Kaßner, A. Stuke, F. Hauler, D. Hathiramani, and D. Stöver, Advanced Thermal Spray Technologies for Applications in Energy Systems, *Surf. Coat. Technol.*, 2008, **202**, p 4432-4437
3. G. Mauer and R. Vaßen, Technology Vision: Current Developments and Challenges in Thermal Barrier Coatings, *Surf. Eng.*, 2011, **27**(7), p 477-479
4. D.J. de Wet, R. Taylor, and F.H. Stott, Corrosion Mechanisms of ZrO_2-Y_2O_3 Thermal Barrier Coatings in the Presence of Molten Middle-East Sand, *J. Phys. IV France*, 1993, **3**, p C9-655-C9-663
5. A. Aygun, A.L. Vasilev, N.P. Padture, and X. Ma, Novel Thermal Barrier Coatings that are Resistant to High-Temperature Attack by Glassy Deposits, *Acta Mater.*, 2007, **55**(20), p 6734-6745
6. S. Krämer, J. Yang, and C.G. Levi, Infiltration-Inhibiting Reaction of Gadolinium Zirconate Thermal Barrier Coatings with CMAS Melts, *J. Am. Ceram. Soc.*, 2008, **91**(2), p 576-583
7. R. Wenglarz and J. Oakey, Gas Turbine Issues in Advanced Gasification Systems, *Materials for Advanced Power Engineering 2006: Proceedings of the 8th Liège Conference*, J. Lecomte-Beckers, M. Carton, F. Schubert, and P.J. Ennis, Ed., Forschungszentrum Jülich, Jülich, 2006
8. P. Mohan, B. Yuan, T. Patterson, V.H. Desai, and Y.H. Sohn, Degradation of Yttria-Stabilized Zirconia Thermal Barrier Coatings by Vanadium Pentoxide, Phosphorous Pentoxide, and Sodium Sulfate, *J. Am. Ceram. Soc.*, 2007, **90**(11), p 3601-3607
9. U. Schulz, B. Saruhan, K. Fritscher, and C. Leyens, Review on Advanced EB-PVD Ceramic Topcoats for TBC Applications, *Int. J. Appl. Ceram. Technol.*, 2004, **1**(4), p 302-315
10. L. Pawlowski, *The Science and Engineering of Thermal Spray Coatings*, 2nd ed., John Wiley & Sons, Chichester, 2008
11. R.B. Heimann, *Plasma Spray Coating*, 2nd ed., Wiley-VCH, Weinheim, 2008
12. R. Vaßen, M.O. Jarligo, T. Steinke, D.E. Mack, and D. Stöver, Overview on Advanced Thermal Barrier Coatings, *Surf. Coat. Technol.*, 2010, **205**, p 938-942
13. A. Kulkarni, A. Vaidya, A. Goland, S. Sampath, and H. Herman, Processing Effects on Porosity-Property Correlations in Plasma Sprayed Yttria-Stabilized Zirconia Coatings, *Mater. Sci. Eng. A*, 2003, **359**, p 100-111
14. A. Feuerstein, J. Knapp, T. Taylor, A. Ashary, A. Bolcavage, and N. Hitchmann, Technical and Economical Aspects of Current Thermal Barrier Coating Systems for Gas Turbine Engines by Thermal Spray and EBPVD: A Review, *J. Therm. Spray Technol.*, 2008, **17**, p 199-213
15. R. Vaßen, A. Stuke, and D. Stöver, Recent Developments in the Field of Thermal Barrier Coatings, *J. Therm. Spray Technol.*, 2009, **18**, p 181-186
16. G. Mauer, R. Vaßen, and D. Stöver, Atmospheric Plasma Spraying of Yttria-Stabilized Zirconia Coatings with Specific Porosity, *Surf. Coat. Technol.*, 2009, **204**, p 172-179
17. M. Karger, R. Vaßen, and D. Stöver, Atmospheric Plasma Sprayed Thermal Barrier Coatings with High Segmentation Crack Densities: Spraying Process, Microstructure and Thermal Cycling Behavior, *Surf. Coat. Technol.*, 2011, **206**, p 16-23
18. U. Schulz, Phase Transformation in EB-PVD Yttria Partially Stabilized Zirconia Thermal Barrier Coatings During Annealing, *J. Am. Ceram. Soc.*, 2000, **83**(4), p 904-910
19. A. Cipitria, I.O. Golosnoy, and T.W. Clyne, A Sintering Model for Plasma-Sprayed Zirconia TBCs. Part I: Free-Standing Coatings, *Acta Mater.*, 2009, **57**(4), p 980-992
20. R. Vassen, X. Cao, F. Tietz, D. Basu, and D. Stöver, Zirconates as New Materials for Thermal Barrier Coatings, *J. Am. Ceram. Soc.*, 2000, **83**(8), p 2023-2028
21. H. Lehmann, D. Pitzer, G. Pracht, R. Vaßen, and D. Stöver, Thermal Conductivity and Thermal Expansion Coefficients of the Lanthanum Rare-Earth-Element Zirconate System, *J. Am. Ceram. Soc.*, 2004, **86**(8), p 1338-1344
22. R. Vaßen, F. Traeger, and D. Stöver, New Thermal Barrier Coatings Based on Pyrochlore/YSZ Double-Layer Systems, *Int. J. Appl. Ceram. Technol.*, 2004, **1**(4), p 351-361
23. X.Q. Cao, R. Vaßen, F. Tietz, and D. Stöver, New Double-Ceramic-Layer Thermal Barrier Coatings Based on Zirconia-Rare Earth Composite Oxides, *J. Eur. Ceram. Soc.*, 2006, **26**, p 247-251
24. R. Vaßen, H. Kaßner, G. Mauer, and D. Stöver, Suspension Plasma Spraying: Process Characterization and Applications, *J. Therm. Spray Technol.*, 2010, **19**(1-2), p 219-225
25. A. Hospach, G. Mauer, R. Vaßen, and D. Stöver, Columnar Structured Thermal Barrier Coatings (TBCs) by Thin Film Low Pressure Plasma Spraying (LPPS-TF), *J. Therm. Spray Technol.*, 2011, **20**(1-2), p 116-120
26. B. Rajasekaran, G. Mauer, and R. Vaßen, Enhanced Characteristics of HVOF Sprayed MCrAlY Bond Coats for TBC Applications, *J. Therm. Spray Technol.*, 2012, **20**(6), p 1209-1216
27. A.V. Radha, S.V. Ushakov, and A. Navrotsky, Thermochemistry of Lanthanum Zirconate Pyrochlore, *J. Mater. Res.*, 2009, **24**(11), p 3350-3357
28. R. Vaßen, Entwicklung neuer oxidischer Wärmedämmschichten für Anwendungen in stationären und Flug-Gasturbinen, Schriften des Forschungszentrums Jülich, *Energy Technology*, vol 33, Forschungszentrum Jülich, Jülich, 2004 (in German)
29. H. Chen, Y. Gaoa, Y. Liua, and H. Luo, Coprecipitation Synthesis and Thermal Conductivity of $La_2Zr_2O_7$, *J. Alloy. Compd.*, 2009, **480**, p 843-848
30. X.Q. Cao, R. Vaßen, W. Jungen, S. Schwartz, F. Tietz, and D. Stöver, Thermal Stability of Lanthanum Zirconate Plasma-Sprayed Coating, *J. Am. Ceram. Soc.*, 2001, **84**(9), p 2086-2090

31. H. Chen, Y. Gao, S. Tao, Y. Liu, and H. Luo, Thermophysical Properties of Lanthanum Zirconate Coating Prepared by Plasma Spraying and the Influence of Post Annealing, *J. Alloy. Compd.*, 2009, **486**, p 391-399
32. Z. Xu, L. He, R. Mu, S. He, and X. Cao, Preparation and Characterization of $La_2Zr_2O_7$ Coating with the Addition of Y_2O_3 by EB-PVD, *J. Alloy. Compd.*, 2010, **492**, p 701-705
33. J.L. Margrave, Ed., *The Characterization of High Temperature Vapors*, Wiley, New York, 1967
34. G. Mauer, D. Sebold, R. Vaßen, and D. Stöver, Improving Atmospheric Plasma Spraying of Zirconate Thermal Barrier Coatings Based on Particle Diagnostics, *J. Therm. Spray Technol.*, 2012, **21**(3-4), p 363-371
35. G. Mauer, R. Vaßen, and D. Stöver, Comparison and Applications of DPV-2000 and Accuraspray-g3 Diagnostic Systems, *J. Therm. Spray Technol.*, 2007, **16**(3), p 414-424
36. W. Braue and P. Mechnich, Recession of an EB-PVD YSZ Coated Turbine Blade by $CaSO_4$ and Fe, Ti-Rich CMAS-Type Deposits, *J. Am. Ceram. Soc.*, 2011, **94**(12), p 4483-4489
37. J.M. Drexler, A.D. Gledhill, K. Shinoda, A.L. Vasiliev, K.M. Reddy, S. Sampath, and N.P. Padture, Jet Engine Coatings for Resisting Volcanic Ash Damage, *Adv. Mater.*, 2011, **23**, p 2419-2424
38. A.D. Gledhill, K.M. Reddy, J.M. Drexler, K. Shinoda, S. Sampath, and N.P. Padture, Mitigation of Damage from Molten Fly Ash to Air-Plasma-Sprayed Thermal Barrier Coatings, *Mater. Sci. Eng. A*, 2011, **528**, p 7214-7221
39. M.O. Jarligo, D.E. Mack, and R. Vaßen, $Gd_2Zr_2O_7$-YSZ Composites for High Temperature Corrosion Resistant Thermal Barrier Coatings, *Abstracts from the 36th International Conference and Exposition on Advanced Ceramics and Composites*, January 22-27, 2012 (Daytona Beach, FL, USA), 2012
40. B. Heimberg, W. Beele, K. Kempter, U. Bast, T. Haubold, M. Hoffmann, A. Endriss, P. Greil, C. Hong, F. Alding, and H. Seifert, ''Process for Producing a Ceramic Thermal Barrier Layer for Gas Turbine Engine Component,'' U.S. Patent 06602553 B2, 2003
41. A.S. Bhalla, R. Guo, and R. Roy, The Perovskite Structure—A Review of Its Role in Ceramic Science and Technology, *Mater. Res. Innov.*, 2000, **4**, p 3-26
42. R. Guo, A.S. Bhalla, and L.E. Cross, $Ba(Mg_{1/3}Ta_{2/3})O_3$ Single Crystal Fiber Grown by the Laser Heated Pedestal Growth Technique, *J. Appl. Phys.*, 1994, **75**, p 4704-4708
43. W. Ma, M.O. Jarligo, D.E. Mack, D. Pitzer, J. Malzbender, R. Vaßen, and D. Stöver, New Generation Perovskite Thermal Barrier Coating Materials, *J. Therm. Spray Technol.*, 2008, **17**(5-6), p 831-837
44. M.O. Jarligo, D.E. Mack, R. Vaßen, and D. Stöver, Application of Plasma Sprayed Complex Perovskites as Thermal Barrier Coatings, *J. Therm. Spray Technol.*, 2009, **18**, p 187-193
45. A. Ansar, G. Schiller, O. Patz, J.B. Gregoire, and Z. Ilhan, Plasma Sprayed Oxygen Electrode for Solid Oxide Fuel Cells and High Temperature Electrolyzers, *Thermal Spray 2008: Crossing Borders*, on CD-ROM, E. Lugscheider, Ed., June 2-4, 2008 (Maastricht, The Netherlands), DVS Media, Düsseldorf, Germany, 2008
46. G. Schiller, M. Müller, and F. Gitzhofer, Preparation of Perovskite Powders and Coatings by Radio Frequency Suspension Plasma Spraying, *J. Therm. Spray Technol.*, 1999, **8**, p 389-392
47. C. Zhang, W.-Y. Li, H. Liao, C.-J. Li, C.-X. Li, and C. Coddet, Microstructure and Electrical Conductivity of Atmospheric Plasma-Sprayed LSM/YSZ Composite Cathode Materials, *J. Therm. Spray Technol.*, 2007, **16**, p 1005-1010
48. M.O. Jarligo, D.E. Mack, G. Mauer, R. Vaßen, and D. Stöver, Atmospheric Plasma Spraying of High Melting Temperature Complex Perovskites for TBC Application, *J. Therm. Spray Technol.*, 2010, **19**(1-2), p 303-310
49. G.V. Samsonov, Ed., *The Oxide Handbook*, 2nd ed., IFI/Plenum, New York, 1986
50. M.O. Jarligo, G. Mauer, D. Sebold, D.E. Mack, R. Vaßen, and D. Stöver, Decomposition of $Ba(Mg_{1/3}Ta_{2/3})O_3$ Perovskite During Atmospheric Plasma Spraying, *Surf. Coat. Technol.*, 2012, **206**(8-9), p 2515-2520
51. G. Mauer, M.O. Jarligo, D.E. Mack, R. Vaßen, and D. Stöver, Development of Plasma Spray Parameters for Ceramic Coatings in Gas Turbines, *Proceedings of the 24th International Conference on Surface Modification Technologies (SMT 24)*, T.S. Sudarshan, E. Beyer, and L.M. Berger, Ed., September 7-9, 2010 (Dresden), Valardocs, Chennai, India, 2011, p 35-46
52. W. Ma, D.E. Mack, R. Vaßen, and D. Stöver, Perovskite-Type Strontium Zirconate as a New Material for Thermal Barrier Coatings, *J. Am. Ceram. Soc.*, 2008, **91**(8), p 2630-2635
53. Y. Zhang, D.E. Mack, M.O. Jarligo, X. Cao, R. Vaßen, and D. Stöver, Partial Evaporation of Strontium Zirconate During Atmospheric Plasma Spraying, *J. Therm. Spray Technol.*, 2009, **18**(4), p 694-701
54. C. Friedrich, R. Gadow, and T. Schirmer, Lanthanum Hexaaluminate—A New Material for Atmospheric Plasma Spraying of Advanced Thermal Barrier Coatings, *J. Therm. Spray Technol.*, 2001, **10**(4), p 592-598
55. C.M. Weyant and K.T. Faber, Processing-Microstructure Relationships for Plasma-Sprayed Yttrium Aluminum Garnet, *Surf. Coat. Technol.*, 2008, **202**(24), p 6081-6089
56. G. Pracht, R. Vaßen, and D. Stöver, Lanthanum-Lithium Hexaaluminate—A New Material for Thermal Barrier Coatings in Magnetoplumbite Structure—Material and Process Development, *Ceram. Eng. Sci. Proc.*, 2008, **27**(3), p 87-99
57. A. Doncieux, D. Stagnol, M. Huger, T. Chotard, C. Gault, T. Ota, and S. Hashimoto, Thermo-Elastic Behaviour of a Natural Quartzite: Itacolumite, *J. Mater. Sci.*, 2008, **43**(12), p 4167-4174
58. T.A. Schaedler, R.M. Leckie, S. Krämer, A.G. Evans, and C.G. Levi, Toughening of Non-transformable t'-YSZ by Addition of Titania, *J. Am. Ceram. Soc.*, 2007, **90**, p 3896-3901
59. M.O. Jarligo, G. Mauer, D.E. Mack, R. Vaßen, and D. Stöver, The Influence of Titania Doping on Plasma-Sprayed YSZ Thermal Barrier Coatings *Proceedings of the 25th International Conference on Surface Modification Technologies (SMT 25)*, T.S. Sudarshan and P. Nylén, Ed., June 20-22, 2011 (Trollhättan, Sweden), Valardocs, 2012, p 165-173
60. T.A. Schaedler, O. Fabrichnaya, and C.G. Levi, Phase Equilibria in the TiO_2-$YO_{1.5}$-ZrO_2 System, *J. Eur. Ceram. Soc.*, 2008, **28**, p 2509-2520
61. M.O. Jarligo, G. Mauer, D.E. Mack, R. Vaßen, and D. Stöver, Advanced Thermal Barrier Coatings from Ti-Doped YSZ Systems, *International Thermal Spray Conference 2011*, Sep 27-29, 2011 (Hamburg, Germany), DVS-Berichte 276, DVS Media, Düsseldorf, Germany, 2011
62. D. Zhu and R.A. Miller, Development of Advanced Low Conductivity Thermal Barrier Coatings, *Int. J. Appl. Ceram. Technol.*, 2004, **1**(1), p 86-94
63. M.O. Jarligo, D.E. Mack, and R. Vaßen, Ti,Yb-Doped YSZ Systems for Advanced Thermal Barrier Coating Applications, *10th CMCEE—International Symposium on Ceramic Materials and Components for Energy and Environmental Applications*, May 20-23, 2012 (Dresden, Germany), 2012